Construction and Building Materials 266 (2021) 121173

Contents lists available at ScienceDirect

Construction and Building Materials

journal homepage: www.elsevier.com/locate/conbuildmat

Development of basalt fiber engineered cementitious composites and its mechanical properties

Mingfeng Xu [a], Song Song [a], Lei Feng [a], Jian Zhou [a,*], Hui Li [a], Victor C. Li [b]

[a] School of Civil and Transportation Engineering, Hebei University of Technology, Tianjin 300401, China
[b] Department of Civil and Environmental Engineering, University of Michigan, Ann Arbor, MI 48109-2125, USA

HIGHLIGHTS

- Basalt fiber-ECC with unique strain-hardening and multiple-cracking behavior has been developed.
- BF-ECC demonstrates an average crack width below 10 μm and crack spacing less than 3 mm.
- The tight and saturated cracks are attributed to the bridging behavior of basalt fiber in matrix.

ARTICLE INFO

Article history:
Received 4 May 2020
Received in revised form 17 September 2020
Accepted 29 September 2020

Keywords:
Basalt fiber
Engineered cementitious composites
Mechanical properties
Crack pattern

ABSTRACT

Fiber plays a key role in the mechanical properties of Engineered Cementitious Composites (ECC), a new generation of fiber-reinforced concrete with excellent ductility and exceptional crack control capability. However, ECC loses its high ductility when exposed to fire, as the synthetic fibers typically used in ECC melt resulting in a loss of crack-bridging ability in elevated temperatures. In this study, the feasibility of using basalt fiber, an inorganic fiber with high-temperature resistance, to develop ECC is investigated experimentally. The results show that basalt fiber reinforced ECC (BF-ECC) exhibits a very unique strain-hardening and multiple-cracking behavior when compared with typical ECCs. The tensile stress–strain curve of BF-ECC is relatively smooth, with average crack width below 10 μm and crack spacing less than 3 mm. The unique features of BF-ECC are interpreted based on the bridging behavior of basalt fibers. This work paves the way for further developing ECC with high-temperature resistance.

1. Introduction

Engineered Cementitious Composites (ECC) has attracted wide interests, as it exhibits unique strain-hardening and multiple-cracking behavior [1]. Under tensile or flexural loading, ordinary concrete experiences a brittle fracture failure mode, and the first crack formation is accompanied by a sudden loss of load carrying capacity [2]. Fiber reinforced concrete exhibits enhanced fracture toughness, but tension-softens after first-cracking [3]. ECC is designed to impart tensile ductility in cementitious materials. Based on micromechanical theory, fiber, matrix, and fiber/matrix interface in ECC are deliberately engineered for synergistic interactions so that load carrying capacity is maintained after first cracking. Hence, ECC strain-hardens to a tensile strain capacity hundreds of times that of normal concrete or fiber reinforced concrete (Fig. 1) [4]. Besides, even at deformation of several percent, the crack width of ECC is self-controlled to below 100 μm [1,3,5]. The high tensile ductility and tight crack width of ECC contributes to infrastructure resilience, durability, and sustainability [1,6–8].

Most ECC developed to date are reinforced with synthetic fibers. Polyethylene (PE) fiber was first introduced to develop ECC in the mid-1990 s [9,10], showing tensile strain capacity over 5%. Recently, owing to its high strength, PE fibers are especially popular in developing ECC with tensile strength over 10 MPa and compressive strength over 100 MPa [11,12]. Contrary to the hydrophobic nature of PE fiber, polyvinyl alcohol (PVA) fiber is hydrophilic due to the presence of the –OH group that leads to a high adhesion with cementitious matrix. Excessive fiber/matrix bond could lead to fiber rupture and loss of crack-bridging ability. Deliberate surface coating (Li [13]) has been effective in moderating the interfacial bond strength and in maintaining the desirable tensile ductility of ECC [14–17]. PVA-ECC has been successfully applied to building, transportation, and water infrastructure [1]. Apart from PE and PVA fiber, polypropylene (PP) fiber has also been used in ECC [18–20]. PP fiber has a relatively lower elastic

* Corresponding author.
E-mail address: zhoujian@hebut.edu.cn (J. Zhou).

https://doi.org/10.1016/j.conbuildmat.2020.121173
0950-0618/

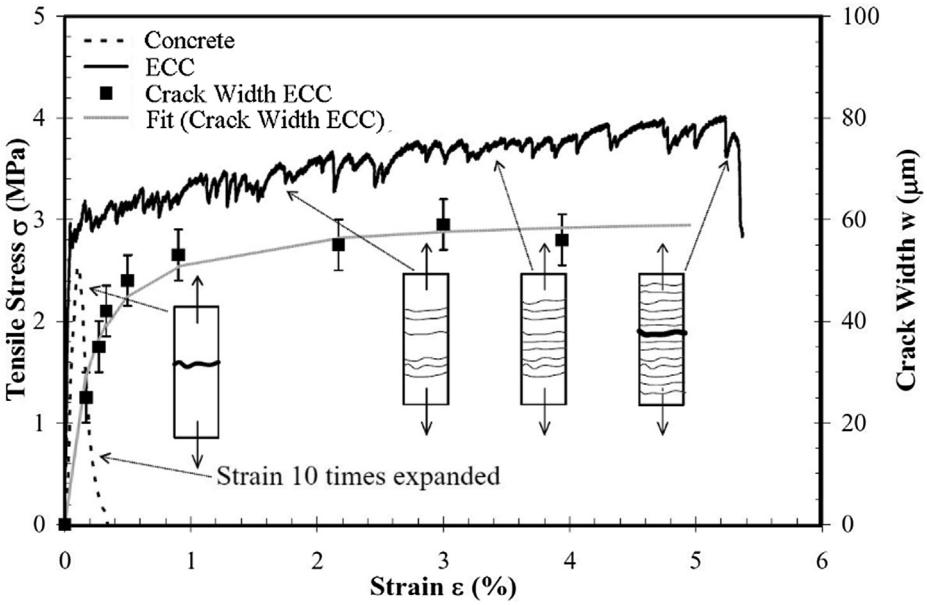

Fig. 1. Typical ECC tensile stress–strain curves and cracking width development curve (modified from [4]).

modulus. The tensile strength of PP-ECC is relatively low (2 MPa) [18]. Recently, poly(p-phenylene-tenephtha) (aramid) and as-spun poly(p-phenylene-2,6-benzobisoxazole) (PBO) fibers were also used to produce high-strength ECC [21] with tensile strength of 10 MPa. In order to improve the greenness and reduce cost, ECC with recycled polyethylene terephthalate (PET) fibers hybrid with PVA fibers have been developed [22]. With 50% replacement of PVA fiber, the PET-PVA hybrid ECC showed a tensile strength over 3.6 MPa and tensile strain of 2.2%.

Fire exposure is one of the most destructive conditions to all concrete structures during their service life. ECC with synthetic fibers demonstrated good fire resistance within a certain range of elevated temperatures. Yu et al [23] found that the compressive properties of PVA-ECC (including stress, strain, stiffness) were retained when subjected to 200 °C. Yu et al [24] reported that the PVA-ECC subjected to 100 °C exhibited better residual tensile ductility and strain-hardening behavior than that without temperature exposure, followed by a slight decline of tensile properties after 200 °C. Under elevated temperature (up to 200 °C), the performance of ECC containing synthetic fibers can be reduced as a result of loss in fiber stiffness, strength, and fiber/matrix interfacial bonding strength. At even higher temperatures (500 °C), complete decomposition of synthetic fiber and loss of composite ductility have been shown [23,25–26]. While synthetic fibers can reduce the fire-induced spalling by releasing the inside water vapor out from the channels of the melted fibers, the performance deterioration of ECC exposed to high temperatures limits its application in fire-sensitive applications. To maintain ductile performance of ECC at elevated temperatures, a new fiber is sought.

Basalt fiber from molten basalt rocks is considered a high-performance green inorganic material. It has attracted attention due to its good physico-chemical properties, eco-compatibility and recyclability [27]. Further, basalt fiber exhibits high thermal stability in a wide range of temperature from – 200 °C to 700 °C [28,29]. Application of basalt fiber in concrete structures as a strengthening material has been studied. Basalt fiber reinforced concrete showed higher strength, better toughness, thermal resistance and impact performance [30–34]. In view of the above, the applicability of the basalt fiber in ECC is anticipated, however, has not yet been studied.

This research aims to investigate the applicability of basalt fiber in ECC. To this end, the Basalt Fiber Engineered Cementitious Composites (BF-ECC) with different amounts of basalt fiber and matrix ingredients were designed. Compressive and uniaxial tensile tests were conducted to characterize the macro-scale mechanical properties. The underlying mechanisms of the crack pattern are investigated from the perspective of *meso*-scale relationship of fiber bridging and crack opening displacement. The focus of the present research is on the development of BF-ECC. The performance of BF-ECC at elevated temperatures is a matter of a future investigation.

2. Experimental program

2.1. Raw materials and mix proportions

The raw materials of BF-ECC include ordinary Portland cement (OPC), fly ash (FA) and silica fume (SF), as binders. Short-cut basalt fiber (BF) (from Shanxi Jintou) was used as the reinforcement material. Polycarboxylate-based high-range water-reducing admixture (HRWRA) was added into the mixture for a good dispersion of BF. The chemical compositions of OPC, FA and SF are listed in Table 1. The physical and mechanical properties of BF are given in Table 2.

The mix proportions of the BF-ECC are given in Table 3. The mixture was designed with three levels of basalt fibers and three levels of cement contents, to explore the feasibility of using BF to develop ECC and to investigate the influence of matrix strength and fiber reinforcement effectiveness on the performance of BF-ECC. In the five mixtures, the content of HRWRA was adjusted until the flowability of the mixtures reached 190 mm ± 5 mm. Flowability test was conducted according to ASTM C 1437 [35].

2.2. Specimen preparation and experimental methods

Dry powder ingredients including the powder HRWRA were put in a plastic bag and mix for 2 min. After hand-dry mixing, they were mixed with water in a 5-Liter mixer at 1 rps for 1 min and then 2 rps for 2 min. Next, fibers were manually added to the mixture and mixed for 5 min until fibers were evenly distributed in the mixture. Immediately after casting, specimens were cured in

Table 1
Chemical compositions of OPC, FA and SF (wt.%).

Materials	SiO_2	Al_2O_3	Fe_2O_3	CaO	MgO	SO_3	TiO_2	LOI	Total
OPC	19.79	5.31	2.88	64.31	2.52	2.47	0.34	1.46	99.08
FA	48.63	37.37	3.78	3.05	1.60	–	–	3.61	98.88
SF	87.28	1.09	0.75	0.87	1.76	1.47	–	4.74	97.96

Table 2
Properties of BF.

Density (g/cm^3)	Tensile strength (MPa)	Elastic modulus (GPa)	Elongation (%)	Length (mm)	Diameter (μm)
2.695	2230	85.8	2.85	9	14.1

Table 3
Mix proportions of BF-ECC (wt.%).

Mixture	OPC	FA	SF	w/b*	HRWRA	BF (vol.%)
M-10-2.0	10	80	10	0.2	0.5	2.0
M-15-2.0	15	75	10	0.2	0.8	2.0
M-20-2.0	20	70	10	0.2	0.9	2.0
M-15-1.5	15	75	10	0.2	0.7	1.5
M-15-3.0	15	75	10	0.2	1.1	3.0

* w/b = water/binder, where the binder materials include OPC, FA and SF.

molds at 20 °C ± 2 °C and 95% ± 5% relative humidity. After 24 h, the specimens were demolded and then cured at 20 °C ± 2 °C and relative humidity of 95% ± 5% until 28 days.

Compressive strength was determined with cube specimens (40 mm × 40 mm) [36]. Six specimens were prepared for each test case. Tensile test was conducted following the same method recommended in both the Chinese standard [37] and the Japanese standard [38]. The dogbone-shaped specimen was used as shown in Fig. 2(a). Fig. 3 illustrates the uniaxial tensile test set up. One extensometer was attached on the specimen to measure the deformation. The test was performed under displacement control at a constant rate of 0.2 mm/min. Six dogbone-shaped specimens were used for each test. The reduced cross-section of dogbone-shaped geometry lead to most cracks occurring in the gauge region, which makes the measurements more reliable [11]. After the test, the crack number and crack spacing was counted, within the gauge length along the central axis by microscope (100 ×). A line was drawn on each specimen as reference line with cracks crossing these lines more or less perpendicularly. Microcracks were measured parallel to the tensile load direction along the reference lines. The average crack number N of each specimen was calculated by averaging the number of cracks on the front and back sides of the specimen. Since ECC deforms several hundred times larger than matrix, the elastic deformation of matrix contributes little to the overall deformation of the composites. Therefore, the overall tensile deformation is considered as the sum of crack openings. Accordingly, the average crack width can be calculated by dividing the tensile deformation at the peak load by the average crack

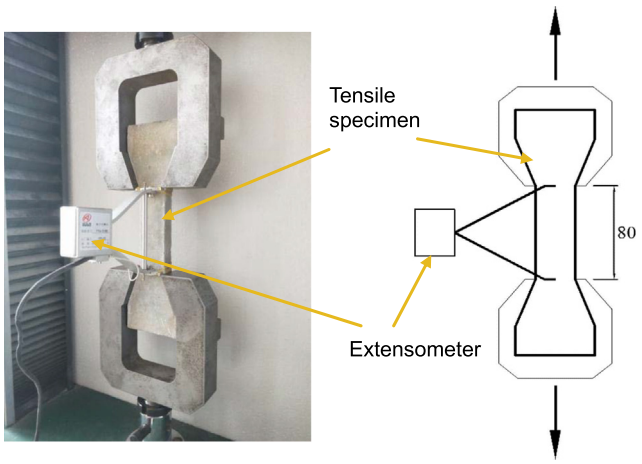

Fig. 3. Uniaxial tensile test set-up (unit: mm).

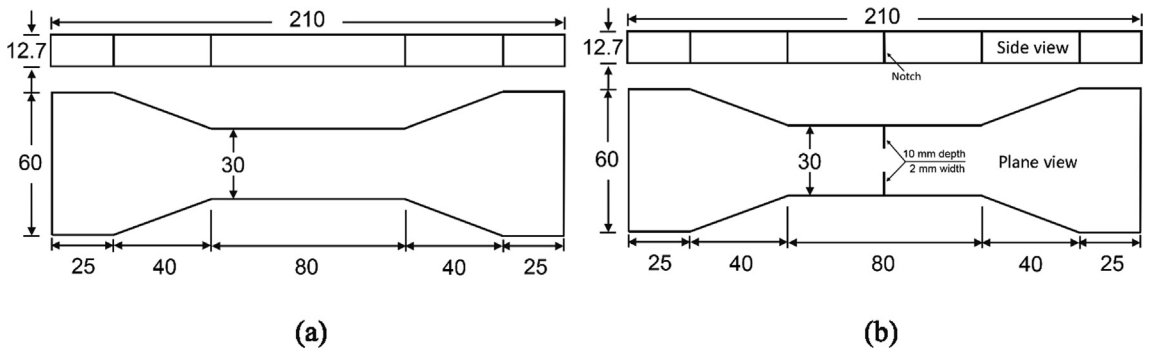

Fig. 2. Dogbone-shaped specimen geometry for: (a) uniaxial tensile test; (b) single crack test with 10 mm-width and 2 mm-width notches on both front and back sides. (unit: mm).

number, and the crack spacing is calculated by dividing the gauge length by the average crack number [16].

For an in-depth understanding of the mechanism behind the crack pattern of the BF-ECC, tensile stress versus crack opening relationship of BF-ECC was determined using a notched dogbone specimen. The notch was cut on each lateral side of the specimen, with notch depth of 10 mm and opening of 2 mm in the middle of the 80 mm gauge (Fig. 2(b)). Six notched dogbone specimens were prepared for each case. Test procedure was the same as that with un-notched dogbone specimen.

A Scanning Electron Microscope (FEI Nova NanoSEM 450 with an accelerated voltage of 15 kV) was used to characterize the microscopic morphology of BF-ECC after loading. 10 mm × 10 mm × 5 mm samples were cut from the tested dogbone specimen, containing the fresh and undestroyed crack section. The sample was coated with a thin layer of carbon conducting film.

3. Results

3.1. Mechanical properties

The compressive strength and tensile properties of BF-ECC are summarized in Table 4. The tensile stress–strain curves of BF-ECCs at the age of 28 days are shown in Fig. 4. The tensile stress is calculated using the measured tensile force and cross-sectional area of the dog-bone specimen within the gauge length; the tensile stress of the point where the slope of the tensile stress–strain curve drops represents the first cracking strength; the maximum tensile stress is defined as the ultimate tensile strength and the corresponding strain is defined as the tensile strain capacity.

The increase of cement content leads to higher compressive strength and hence stronger composites. However, as the fiber volume increases from 1.5% to 3.0%, the compressive strengths of BF-ECC show little difference and range from 23.3 MPa to 25.4 MPa, indicating that the compressive strength does not seem to be significantly affected by the fiber content. This phenomenon is consistent with previous findings [27,39].

All the ECC specimens prepared with basalt fiber exhibit strain-hardening characteristics under uniaxial tensile stress. After first cracking, a subsequent increase in tensile stress was followed. At the fixed fiber content of 2.0%, as the cement content increases from 10% to 20%, the first cracking strength increases from 1.86 MPa to 2.44 MPa and the ultimate tensile strength increases from 3.29 MPa to 3.51 MPa. Conversely, tensile strain capacity shows a continuous drop with increase with cement content. This trend is consistent with ECC prepared with PVA fibers [15,40]. When fly ash with less hydration activity replaces cement, it tends to reduce the fiber/matrix interfacial bond and matrix toughness [40]. As the matrix fracture toughness governs the cracking stress of the matrix (Irwin's fracture criterion), the higher fracture toughness resulted from the increase of cement and decrease of fly ash content leads to a higher first cracking strength and a reduction in the margin between first cracking and maximum fiber bridging capacity. Also, the strengthening of fiber/matrix interface by high cement content could also lead to fiber rupture [40]. Therefore, BF-ECC with less cement and more fly ash attains higher tensile strain capacity.

High BF volume greatly benefits the strain-hardening behavior, with both increased ultimate tensile strength and tensile strain capacity. Employing 3.0% volume fraction of BF produced a ECC with an ultimate tensile strength of approximately 4.82 MPa and tensile strain capacity of 0.85%, which are 48% and 81% higher than employing 1.5% volume fraction, respectively. The higher fiber volume fraction contributes to the increase of fiber bridging capacity that favors the ultimate tensile strength and tensile strain capacity.

It is worth noting that the tensile strain capacity of BF-ECC in this research ranging from 0.4% to 0.9% is several ten times higher than normal concrete, while it is an order of magnitude lower than ECCs with synthetic fibers.

3.2. Crack width

The crack pattern of the BF-ECC after uniaxial tension is shown in Fig. 5. As most of the cracks are invisible to the naked eyes, the specimen surface was wetted with a wet paper tower to increase the contrast between the cracked and uncracked region. It can be seen that extremely tight cracks are densely distributed (Fig. 5 (a)). Inside the crack section, cracks of several microns are found, and basalt fiber is located crossing the cracks, as shown in Fig. 5 (b). The average crack width and crack spacing of BF-ECC are summarized in Table 4. The average crack width of BF-ECC is 8.38 μm, with spacing averaging 2.22 mm.

4. Discussion

4.1. Tight crack width

Comparison of the average crack width and crack spacing between BF-ECC and previously reported ECCs with PVA fiber [17,41–44], PP fiber [19], and PE fiber [45,46] is summarized in Fig. 6. The crack widths of BF-ECC is an order of magnitude smaller than the typical PVA-ECC, PP-ECC and PE-ECC developed in previous works. The crack spacings of BF-ECC is comparable to that of PP-ECC and PE-ECC and denser than that of most PVA-ECC. With tighter crack width, BF-ECC would be more beneficial for the enhanced durability as well as for extended service life.

To investigate the mechanism on the tight crack width of BF-ECC, single crack test was conducted. A low 0.5% basalt fiber content was incorporated in the mixture to deliberately suppress the multiple cracking tendency intrinsic in ECC. With lower fiber volume, the bridging strength will proportionally decrease while the crack opening at peak load stays the same [1]. The experimentally obtained $\sigma(\delta)$ curve reflects the relationship between the single-crack bridging stress and crack mouth opening displacement (CMOD).

The $\sigma(\delta)$ curves of BF-ECC is depicted in Fig. 7(a). In the $\sigma(\delta)$ curve, the peak stress is named as maximum fiber bridging strength σ_0 and the crack opening corresponding to σ_0 is defined

Table 4
Compressive strength and tensile properties of BF-ECC at the age of 28 days.

Mixture	Compressive strength (MPa)	First cracking strength (MPa)	Tensile strength (MPa)	Tensile strain capacity (%)	Average width of crack (μm)	Average crack pacing (mm)
M-10-2.0	18.1 ± 1.8	1.86 ± 0.11	3.29 ± 0.06	0.73 ± 0.02	6.03	1.10
M-15-2.0	24.0 ± 0.8	2.26 ± 0.14	3.51 ± 0.20	0.61 ± 0.04	7.08	1.21
M-20-2.0	27.7 ± 1.6	2.44 ± 0.08	3.52 ± 0.11	0.42 ± 0.01	8.38	2.22
M-15-1.5	25.4 ± 1.9	2.40 ± 0.30	3.29 ± 0.07	0.48 ± 0.02	6.52	1.78
M-15-2.0	24.0 ± 0.8	2.26 ± 0.14	3.51 ± 0.20	0.61 ± 0.04	7.08	1.21
M-15-3.0	23.3 ± 2.1	2.23 ± 0.18	4.82 ± 0.09	0.85 ± 0.02	6.59	1.05

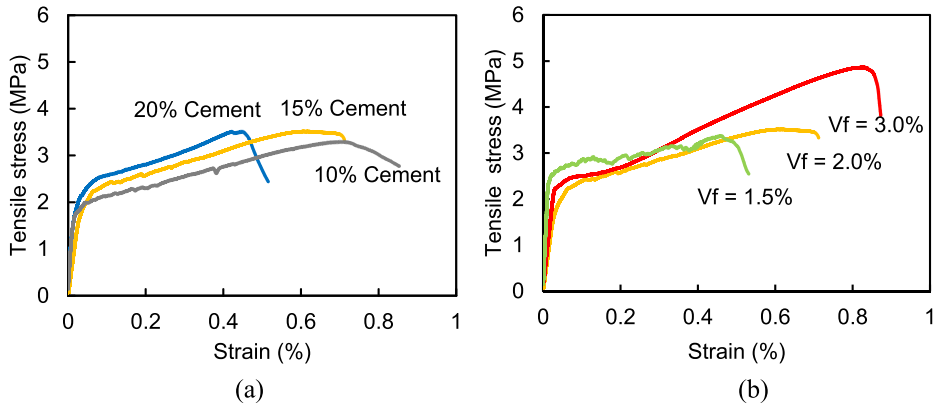

Fig. 4. Tensile stress–strain curves of BF-ECCs at the age of 28 days: (a) BF-ECCs with 10%–20% cement, (b) BF-ECCs with 1.5%–3.0% basalt fiber.

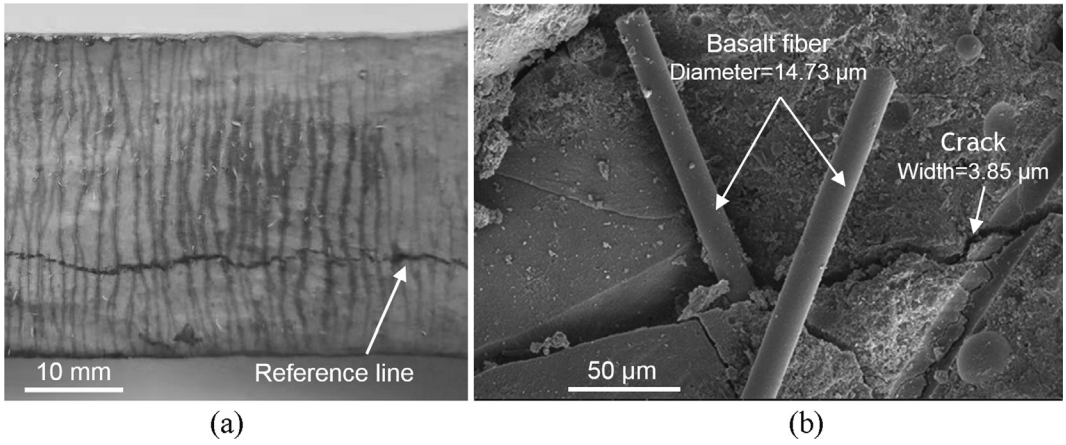

Fig. 5. Crack pattern of BF-ECC with 15% cement and 3.0% fiber after uniaxial tension test: (a) saturated multiple-cracking with tight width under optical microscopy; (b) tight crack width under SEM.

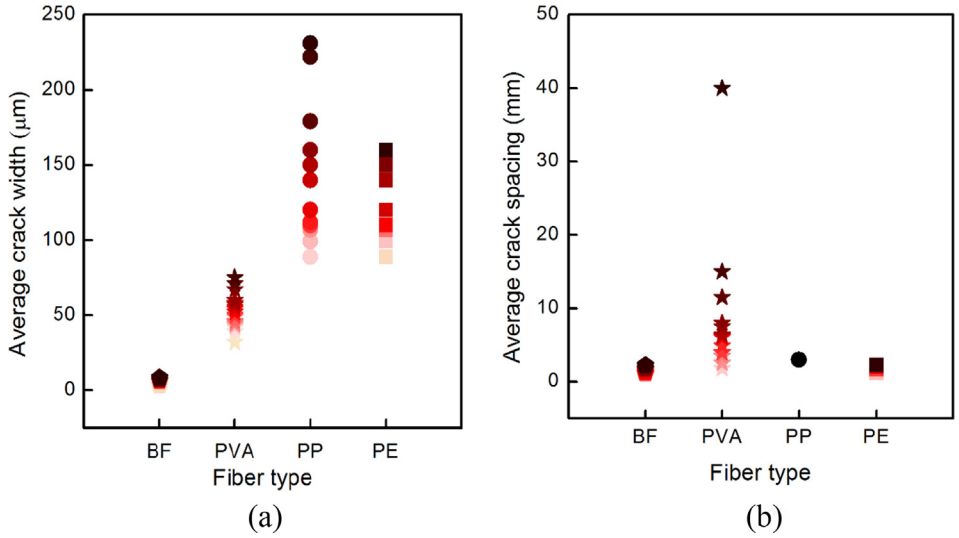

Fig. 6. Comparison on the crack pattern of BF-ECC, PVA-ECC [17,41–44], PP-ECC [19], and PE-ECC [45,46]: (a) average crack with; (b) average crack spacing.

as δ_0. While σ_0 generally increases with fiber content, δ_0 appears less sensitive to fiber content. As comparison, the $\sigma(\delta)$ curves of PVA-ECC in reference [18] are also shown in Fig. 7(b). δ_0 of BF-ECC is 0.039 mm, apparently lower than that of PVA-ECC (0.4 mm). This phenomenon is also true for various matrix or fiber features listed in Table 5.

The reason for the relatively small δ_0 of BF-ECC perhaps lies in the higher stiffness and shear stiffness of BF fibers which behaves

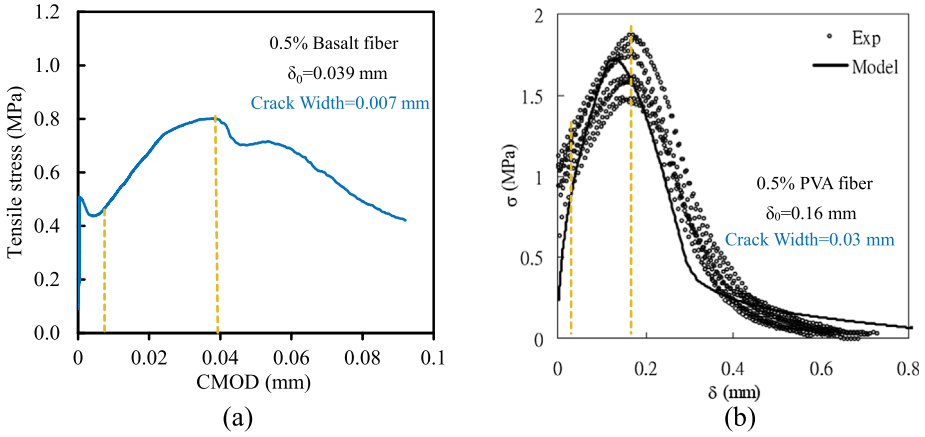

Fig. 7. Experiment stress-CMOD curves (σ(δ)) obtained from notched tensile specimens for: (a) BF-ECC; (b) PVA-ECC [18].

elastic-brittle when compared with synthetic fibers, as well as the high chemical bonding at the fiber/matrix interface. Specifically, research found that the chemical bond of basalt fiber with the cementitious matrix is 1.88 times higher than that of PVA fibers, and the strength reduction coefficients of the basalt fiber due to its brittle behavior were nine times higher than those of the PVA fiber [48]. It is known that final failure occurs at the crack plane with the minimum σ_0. So, when the specimen fails, only the width of the failure crack reaches δ_0, while the other cracks exhibit width smaller than δ_0. It can be inferred that the smaller δ_0 of BF-ECC tends to result in the tighter crack width observed. Further, as the tensile strain capacity is the sum of each crack width, the small δ_0 of BF-ECC limits its tensile strain capacity as large as the ECC with PVA or PE fibers.

4.2. Fluctuation of the tensile stress–strain curve

Comparing the tensile stress–strain curve of BF-ECC with PVA-ECC in reference [17], it is interesting to see that the curve of BF-ECC is smoother than that of PVA-ECC (Fig. 8). The fluctuations represent stress drops associated with the formation of each of the multiple cracks in the uniaxial tensile specimens. Factors that governs the magnitude of stress drops are discussed below.

In a unit section (length = l) of a specimen under tensile stress σ (Fig. 9), a crack is formed at the moment t. The deformation Δl_t in the unit section includes the elastic deformation of part 1 (Δl_{tc}^1), elastic deformation of part 2 (Δl_{tc}^2) and crack width W, as shown in Eqn (3). Correspondingly, before cracking, the stress σ can be expressed by Eqn (4); after cracking, the stress σ_c can be expressed by Eqn (5).

$$\Delta l_t = \Delta l_{tc}^1 + \Delta l_{tc}^2 + w = \Delta l_{tc} + w \tag{3}$$

$$\sigma = \frac{\Delta l_t^1}{l/2} \times E = \frac{\Delta l_t^2}{l/2} \times E = \frac{\Delta l_t}{l} \times E \tag{4}$$

$$\sigma_c = \frac{\Delta l_{tc}^1}{l/2} \times E = \frac{\Delta l_{tc}^2}{l/2} \times E \tag{5}$$

where E is the elasticity modulus of matrix and considered to be constant before and after cracking. It is assumed that all the components including fiber and pre-existing flaws in the matrix distribute uniformly. Therefore, $\Delta l_t{}^1 = \Delta l_t{}^2$ and $\Delta l_{tc}^1 = \Delta l_{tc}^2$. Then Eqn (5) can be transformed as Eqn (6), and the sudden stress drop before and after cracking can be expressed as Eqn (7).

$$\sigma_c = E \times \frac{\Delta l_t - W}{l} \tag{6}$$

$$\Delta\sigma = \sigma - \sigma_c = \frac{\Delta l_t}{l} \times E - \frac{\Delta l_t - W}{l} = \frac{E}{l} \times W \tag{7}$$

From Eqn (7), it can be seen that the stress drop $\Delta\sigma$ of the stress–strain curve is linearly proportional to the crack width W. ECC with larger crack width gives rise to a higher stress drop when a microcrack is generated. Since BF-ECC exhibits tighter cracks than PVA-ECC, PE-ECC or PP-ECC (Table 5), the stress drop associated with each microcrack during strain-hardening is relatively small and the tensile stress–strain curve is smooth without obvious fluctuation.

5. Conclusions

This paper reports the development of BF-ECC and the investigation of its mechanical properties. Based on the experimental results in this study, the following conclusions can be drawn:

- It is feasible to use BF to produce ECC. All BF-ECC specimens investigated exhibit strain-hardening and multiple-cracking characteristics under uniaxial tensile loading. However, the tensile strain capacity of BF-ECC (0.4–0.9%), while at least one order of magnitude higher than normal concrete, is an order of magnitude lower than ECCs reinforced with synthetic fibers (2–5%).

Table 5
Experimental δ_0 of BF-ECC (this research) and PVA-ECC, PP-ECC and PE-ECC from previous literature.

Reference	Fiber	δ_0 (mm)	Crack Width (mm)	Crack Width / δ_0
This research	Basalt	0.039	0.007	0.18
Yang et al, 2008 [18]	PVA	0.16	0.03	0.19
Ranade et al, 2014 [17]	PVA	0.25/0.5	0.057/0.075	0.23/0.15
Pereira et al, 2012 [47]	PP	0.5	–	–
Ranade et al, 2013 [11]	PE	0.25	–	–

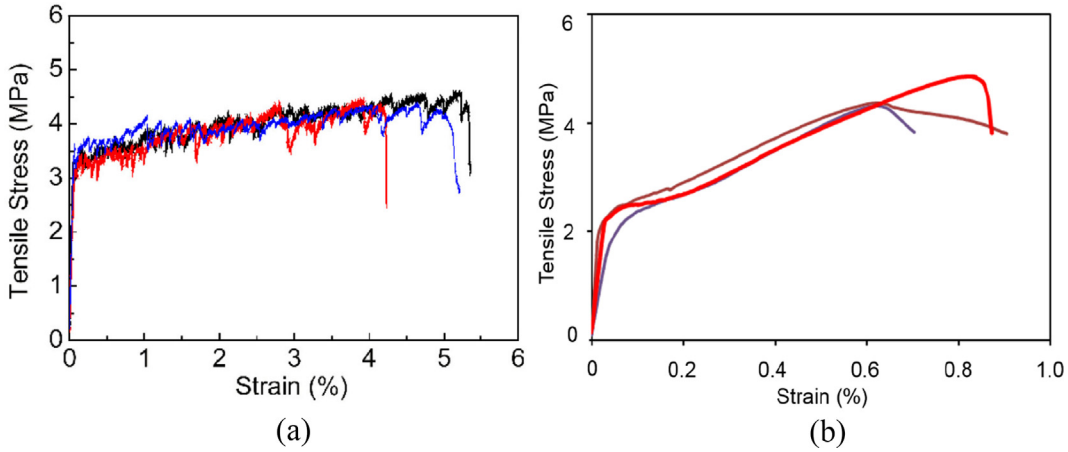

Fig. 8. Comparison on tensile stress–strain curves of (a) PVA-ECC [6] and (b) BF-ECC.

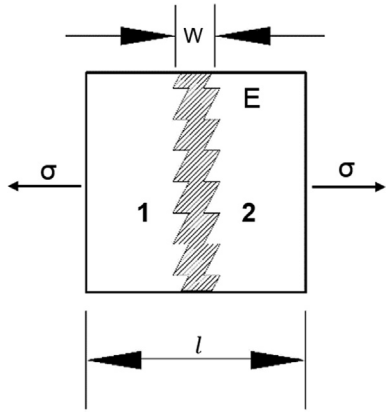

Fig. 9. Schematic diagram showing a unit section (section length = l) from a specimen under tension.

- Extremely tight and densely distributed cracks are exhibited on BF-ECC specimens after tensioning into the strain-hardening regime. The average crack width is less than 8 μm, about one order of magnitude smaller than typical ECCs prepared with PVA, PP or PE fibers.
- The tensile stress–strain curve of BF-ECC is uniquely smooth. Stress drops during strain-hardening in ECC is found to scale linearly with crack width. The almost imperceptible stress drops in BF-ECC is due to its extremely tight crack width.
- Increasing cement content (from 10% to 20%) in the studied BF-ECC leads to an increase in the first cracking strength of (from 1.86 MPa to 2.44 MPa) and the ultimate tensile strength (from 3.29 MPa to 3.51 MPa), but a decrease in the tensile strain capacity. As expected, the ultimate tensile strength and tensile strain capacity of BF-ECC both increase with fiber content.

While this research establishes the feasibility of adopting inorganic basalt fiber in the development of ECC with moderate strain capacity, additional research is needed to investigate the behavior of BF-ECC under elevated temperature.

CRediT authorship contribution statement

Mingfeng Xu: Conceptualization, Methodology, Formal analysis, Data curation, Writing - original draft. **Song Song:** Investigation. **Lei Feng:** Validation. **Jian Zhou:** Supervision, Funding acquisition. **Hui Li:** Writing - review & editing. **Victor C. Li:** Writing - review & editing, Supervision.

Declaration of Competing Interest

The authors declare that they have no known competing financial interests or personal relationships that could have appeared to influence the work reported in this paper.

Acknowledgement

The authors gratefully acknowledge the financial support of Natural Science Foundation of China (No. 51702082, 51878238).

References

[1] V.C. Li, Engineered Cementitious Composites (ECC): Bendable Concrete for Sustainable and Resilient Infrastructure, Springer, 2019.
[2] V.C. Li, Tailoring ECC for special attributes: A review, International Journal of Concrete, Structures and Materials 6 (3) (2012) 135–144.
[3] M. Şahmaran, V.C. Li, Durability of mechanically loaded engineered cementitious composites under highly alkaline environments, Cem. Concr. Compos. 30 (2) (2008) 72–81.
[4] M. Weimann, V.C. Li, Hygral Behavior of Engineered Cementitious Composites (ECC), International Journal for Restoration of Buildings and Monuments 9 (2003) 513–534.
[5] V.C. Li, Engineered cementitious composites (ECC)–material, structural, and durability performance, Concrete Construction Engineering Handbook (2008) 1–78.
[6] V.C. Li, On engineered cementitious composites (ECC), J. Adv. Concr. Technol. 1 (3) (2003) 215–230.
[7] H. Liu, Q. Zhang, V.C. Li, H. Su, C. Gu, Durability study on engineered cementitious composites (ECC) under sulfate and chloride environment, Constr. Build. Mater. 133 (2017) 171–181.
[8] M.D. Lepech, V.C. Li, Long Term Durability Performance of Engineered Cementitious Composites/Langzeitbeständigkeit systematisch entwickelter zusammengesetzter Zement gebundener Werkstoffe, Restoration of Buildings and Monuments 12 (2) (2006) 119–132.
[9] V.C. Li, From micromechanics to structural engineering-the design of cementitous composites for civil engineering applications, JSCE Journal of Structural Mechanics and Earthquake Engineering. 10 (2) (1993) 37–48.
[10] V.C. Li, D.K. Mishra, H.-C. Wu, Matrix design for pseudo-strain-hardening fibre reinforced cementitious composites, Mater. Struct. 28 (10) (1995) 586–595.
[11] R. Ranade, V.C. Li, M.D. Stults, T.S. Rushing, J. Roth, W.F. Heard, Micromechanics of high-strength, high-ductility concrete, ACI Mater. J. 110 (4) (2013) 375–384.
[12] K. Yu, J. Yu, J. Dai, Z. Lu, S.P. Shah, Development of ultra-high performance engineered cementitious composites using polyethylene (PE) fibers, Constr. Build. Mater. 158 (2018) 217–227.
[13] V.C. Li, C. Wu, S. Wang, A. Ogawa, T. Saito, Interface tailoring for strain-hardening polyvinyl alcohol-Engineered Cementitious Composite, ACI Mater. J. 99 (5) (2002) 463–472.
[14] C. Redon, V.C. Li, C. Wu, H. Hoshiro, T. Saito, A. Ogawa, Measuring and modifying interface properties of PVA fibers in ECC matrix, J. Mater. Civ. Eng. 13 (6) (2001) 399–406.

[15] E.-H. Yang, Y. Yang, V.C. Li, Use of high volumes of fly ash to improve ECC mechanical properties and material greenness, ACI Mater. J. 104 (6) (2007) 620–628.
[16] J. Zhou, S. Qian, M.G.S. Beltran, G. Ye, K. van Breugel, V.C. Li, Development of engineered cementitious composites with limestone powder and blast furnace slag, Mater. Struct. 43 (6) (2010) 803–814.
[17] R. Ranade, J. Zhang, J.P. Lynch, V.C. Li, Influence of micro-cracking on the composite resistivity of engineered cementitious composites, Cem. Concr. Res. 58 (2014) 1–12.
[18] E.-H. Yang, Designing added functions in engineered cementitious composites, University of Michigan, Ann Arbor, 2008.
[19] B. Felekoglu, K. Tosun-Felekoglu, R. Ranade, Q. Zhang, V.C. Li, Influence of matrix flowability, fiber mixing procedure, and curing conditions on the mechanical performance of HTPP-ECC, Compos. B Eng. 60 (2014) 359–370.
[20] K. Tosun-Felekoğlu, E. Gödek, M. Keskinateş, B. Felekoğlu, Utilization and selection of proper fly ash in cost effective green HTPP-ECC design, J. Cleaner Prod. 149 (2017) 557–568.
[21] I. Curosu, M. Liebscher, V. Mechtcherine, C. Bellmann, S. Michel, Tensile behavior of high-strength strain-hardening cement-based composites (HS-SHCC) made with high-performance polyethylene, aramid and PBO fibers, Cem. Concr. Res. 98 (2017) 71–81.
[22] J. Yu, J. Yao, X. Lin, H. Li, J.Y.K. Lam, C.K.Y. Leung, I.M.L. Sham, K. Shih, Tensile performance of sustainable Strain-Hardening Cementitious Composites with hybrid PVA and recycled PET fibers, Cem. Concr. Res. 107 (2018) 110–123.
[23] K. Yu, J. Dai, Z. Lu, C.K.Y. Leung, Mechanical properties of engineered cementitious composites subjected to elevated temperatures, J. Mater. Civ. Eng. 27 (10) (2015) 04014268.
[24] J. Yu, J. Lin, Z. Zhang, V.C. Li, Mechanical performance of ECC with high-volume fly ash after sub-elevated temperatures, Constr. Build. Mater. 99 (2015) 82–89.
[25] M. Şahmaran, E. Özbay, H.E. Yücel, M. Lachemi, V.C. Li, Effect of fly ash and PVA fiber on microstructural damage and residual properties of engineered cementitious composites exposed to high temperatures, J. Mater. Civ. Eng. 23 (12) (2011) 1735–1745.
[26] P.S. Bhat, V. Chang, M. Li, Effect of elevated temperature on strain-hardening engineered cementitious composites, Constr. Build. Mater. 69 (2014) 370–380.
[27] E. Monaldo, F. Nerilli, G. Vairo, Basalt-based fiber-reinforced materials and structural applications in civil engineering, Compos. Struct. 214 (2019) 246–263.
[28] J. Sim, C. Park, D.Y. Moon, Characteristics of basalt fiber as a strengthening material for concrete structures, Compos. B Eng. 36 (6) (2005) 504–512.
[29] S. Ying, X. Zhou, Chemical and thermal resistance of basalt fiber in inclement environments, Journal of Wuhan University of Technology 28 (3) (2013) 560–565.
[30] P.C. Chidighikaobi, Thermal effect on the flexural strength of expanded clay lightweight basalt fiber reinforced concrete, Mater. Today:. Proc. (2019).
[31] N. Kabay, Abrasion resistance and fracture energy of concretes with basalt fiber, Constr. Build. Mater. 50 (2014) 95–101.
[32] J. Branston, S. Das, S.Y. Kenno, C. Taylor, Mechanical behaviour of basalt fibre reinforced concrete, Constr. Build. Mater. 124 (2016) 878–886.
[33] D.P. Dias, C. Thaumaturgo, Fracture toughness of geopolymeric concretes reinforced with basalt fibers, Cem. Concr. Compos. 27 (1) (2005) 49–54.
[34] C. Jiang, K. Fan, F. Wu, D. Chen, Experimental study on the mechanical properties and microstructure of chopped basalt fibre reinforced concrete, Mater. Des. 58 (2014) 187–193.
[35] ASTM C 1437. Standard test method for flow of hydraulic cement mortar, West Conshohocken, PA. , 2015.
[36] GB, T, 17671. Method of testing cements-determination of strength 1999 China Standardization Press Beijing, China
[37] JC/T 2641-2018. Standard test method for the mechanical properties of ductile fiber reinforced cementitious composites, Beijing, China Building Materials Press, 2018.
[38] J.C. Committee, Recommendations for design and construction of high performance fiber reinforced cement composites with multiple fine cracks, Japan Society of Civil Engineers, Tokyo, Japan, 2008.
[39] H. Mazaheripour, S. Ghanbarpour, S.H. Mirmoradi, I. Hosseinpour, The effect of polypropylene fibers on the properties of fresh and hardened lightweight self-compacting concrete, Constr. Build. Mater. 25 (1) (2011) 351–358.
[40] S. Wang, V.C. Li, Engineered cementitious composites with high-volume fly ash, ACI Mater. J. 104 (3) (2007) 233–241.
[41] H. Liu, Q. Zhang, C. Gu, H. Su, V.C. Li, Influence of micro-cracking on the permeability of engineered cementitious composites, Cem. Concr. Compos. 72 (2016) 104–113.
[42] E.-H. Yang, S. Wang, Y. Yang, V.C. Li, Fiber-bridging constitutive law of engineered cementitious composites, J. Adv. Concr. Technol. 6 (1) (2008) 181–193.
[43] V.C. Li, C. Wu, S. Wang, A. Ogawa, T. Saito, Interface tailoring for strain-hardening polyvinyl alcohol-engineered cementitious composite (PVA-ECC), ACI Mater. J. 99 (5) (2002) 463–472.
[44] V.C. Li, S. Wang, C. Wu, Tensile strain-hardening behavior or polyvinyl alcohol engineered cementitious composite (PVA-ECC), ACI Mater. J. 98 (2001) 483–492.
[45] J.-I. Choi, B.Y. Lee, R. Ranade, V.C. Li, Y. Lee, Ultra-high-ductile behavior of a polyethylene fiber-reinforced alkali-activated slag-based composite, Cem. Concr. Compos. 70 (2016) 153–158.
[46] R. Ranade, V.C. Li, W.F. Heard, Tensile Rate Effects in High Strength-High Ductility Concrete, Cem. Concr. Res. 68 (2015) 94–104.
[47] E.B. Pereira, G. Fischer, J.A. Barros, Direct assessment of tensile stress-crack opening behavior of Strain Hardening Cementitious Composites (SHCC), Cem. Concr. Res. 42 (6) (2012) 834–846.
[48] J.-I. Choi, B.Y. Lee, Bonding Properties of Basalt Fiber and Strength Reduction According to Fiber Orientation, Materials 8 (10) (2015) 6719–6727.